

An optimized pipeline for functional connectivity analysis in the rat brain

Yujian Diao¹, Ting Yin², Rolf Gruetter^{1,2} and Ileana O. Jelescu^{2,*}

¹Laboratoire d'Imagerie Fonctionnelle et Métabolique, EPFL, Lausanne Switzerland, ²Centre d'Imagerie Biomédicale, EPFL, Lausanne, Switzerland.

Abstract

Resting state functional MRI (rs-fMRI) is a widespread and powerful tool for investigating functional connectivity (FC) and brain disorders. However, FC analysis can be seriously affected by random and structured noise from non-neural sources such as physiology. Thus, it is essential to first reduce thermal noise and then correctly identify and remove non-neural artefacts from rs-fMRI signals through proper data processing methods. However, existing tools that correct for these effects are tailored for human brain and are not readily transposable to rat data. Here, we established a data processing pipeline that can robustly remove random and structured noise from rat rs-fMRI data. It includes a novel denoising approach based on Marchenko-Pastur Principle Component Analysis (MP-PCA) method, FMRIB's ICA-based Xnoiseifier (FIX) for automatic artefact classification and cleaning, and global signal regression (GSR). Our results show that: I) MP-PCA denoising substantially improves the temporal signal-to-noise ratio; II) the pre-trained FIX classifier achieves a high accuracy in artefact classification; III) both artefact cleaning and GSR are essential steps in minimizing the within-group variability in control animals and identifying FC changes in a rat model of sporadic Alzheimer's disease, as compared to controls.

* Corresponding author: Dr. Ileana Jelescu, ileana.jelescu@epfl.ch

1. Introduction

Resting-state fMRI (rs-fMRI), based on spontaneous low-frequency fluctuations in the blood oxygen level dependent (BOLD) signal in the resting brain, is a widely used non-invasive tool for studying intrinsic functional organization in health and disease (Fornito and Bullmore, 2010; Fox and Raichle, 2007). By examining spatio-temporal correlation of BOLD signal between distinct brain regions, known as functional connectivity (FC), this technique is capable of revealing large-scale resting state networks (RSNs) (Biswal et al., 1995; Buckner et al., 2013; Damoiseaux et al., 2006). Nowadays, rs-fMRI has become an increasingly important translational neuroimaging tool for understanding neurological and psychiatric diseases and for developing treatments, with rapidly growing applications not only in human research but also in rodent models of disease (Bajic et al., 2017; Fox and Greicius, 2010).

However, the BOLD signal is contaminated by multiple physiological and non-physiological sources of noise, such as respiratory and cardiac cycles, thermal noise, changes in blood pressure, and head motion (Birn, 2012; Kruger and Glover, 2001; Murphy et al., 2013; Van Dijk et al., 2012). These non-neuronal sources can severely corrupt rs-fMRI time series and thereby confound the FC analysis (Cole et al., 2010; Power et al., 2014). Therefore, a robust pre-processing pipeline is required to extract the neuronal component of BOLD signal and minimize the contribution of noise sources. Furthermore, existing tools that correct for the effect of non-neuronal sources are mostly tailored for human rs-fMRI data and are not readily transposable, or even applicable, to rodent data. Dedicated pipelines and “cookbooks” for rodent rs-fMRI processing are just starting to emerge (Bajic et al., 2017; Zerbi et al., 2015).

For example, model-based approaches such as general linear model (GLM) can estimate and remove BOLD fluctuations resulting from respiratory and cardiac cycles by recording the physiology and modelling these external confounds as regressors in a GLM (Birn et al., 2006; Kasper et al., 2017). While physiological recordings in rodents are possible, they typically involve dedicated hardware and invasive procedures, making them experimentally impractical. However, although cardiac and respiratory frequencies in rodents are much higher than those of the resting-state BOLD fluctuations, depending on the temporal resolution of the acquisition, they can alias back as a lower frequency within the band of interest (typically 0.01 – 0.3 Hz) and corrupt the analysis. Two complementary approaches are therefore suitable to mitigate the impact of physiological noise in resting-state rodent fMRI.

One approach is the removal of global signal (GS) defined as the mean time series averaged over all voxels within the brain by including the GS as a nuisance regressor in GLM analyses, which is referred to as global signal regression (GSR) (Liu et al., 2017). However, the use of GSR has been one of the most controversial topics in human rs-fMRI connectivity studies (Liu et al., 2017; Murphy and Fox, 2017). On the one hand, GSR is known to

introduce spurious negative correlations (Murphy et al., 2009) and cause spatial bias on connectivity measures (Saad et al., 2012). On the other hand, prior studies have shown that GSR can enhance the detection of significant functional connectivity and improve spatial specificity of positive correlations (Fox et al., 2009). Most importantly for rodent studies, GSR can also mitigate confounds related to motion and physiological processes (Aquino et al., 2019; Power et al., 2015).

Another commonly used data-driven approach which identifies various physiological noise components directly from the fMRI data itself is single-level independent component analysis (ICA) (Bajic et al., 2017a; Caballero-Gaudes and Reynolds, 2017; Griffanti et al., 2014; McKeown et al., 2003). The ICA method is also confronted by several issues including model order (i.e. the number of components) selection (Kuang et al., 2018) and the identification of artefactual components which is a manually tedious step (Wang and Li, 2015) especially for a high model order. Notably, a machine-learning approach for automatic artefact component classification based on FMRIB's ICA-based Xnoiseifier (FIX) (Salimi-Khorshidi et al., 2014) has been proposed to replace manual classification. The FIX auto-classifier applied in human and mice rs-fMRI studies has yielded promising results with a high accuracy in artefact identification (Griffanti et al., 2015, 2014; Zerbi et al., 2015). However, the success of FIX classification relies on a proper pre-training on study-specific datasets.

Here, we propose a data processing pipeline for rat rs-fMRI that minimizes intra-group variability and maximizes inter-group differences in whole-brain functional connectivity. In this pipeline, we reduce structural noise by combining single-session ICA cleaning and GSR. For ICA cleaning, we build and use a dedicated FIX classifier for rats. Furthermore, we also enhance the sensitivity to BOLD fluctuations by first increasing dramatically the temporal SNR of the data. For the purpose of stochastic (thermal) noise removal, we employ a novel method based on Marchenko-Pastur Principle Component Analysis (MP-PCA) MP-PCA denoising was recently introduced for diffusion MRI and is a model-free method that exploits redundancy in MRI series (Veraart et al., 2016), which has shown great potential for improving the SNR in other MRI techniques as well (Ades-Aron et al., 2019, 2018; Does et al., 2019).

2. Materials and Methods

2.1. Animal preparation and anesthesia

All experiments were approved by the local Service for Veterinary Affairs. Male Wistar rats (236 ± 11 g) underwent a bilateral icv-injection of either streptozotocin (3 mg/kg, STZ group) or buffer (control group). When delivered exclusively to the brain, streptozotocin induces impaired brain glucose metabolism and is used as a model of sporadic Alzheimer's disease (Grieb, 2016; Knezovic et al., 2015; Lester-Coll et al., 2006).

The fMRI data were acquired on 17 rats in two groups, disease group (STZ, 9 rats) and control group (CTL, 8 rats), at 2, 6, 13 and 21 weeks after the surgery, illustrated in **Figure 1**. Rats were anesthetized using 2% isoflurane in a mixture of O₂ and Air (O₂/Air: 30/70) during initial setup and promptly switched to medetomidine sedation delivered through a subcutaneous catheter in the back (bolus: 0.1mg/kg, perfusion: 0.1mg/kg/h) as previously described (Reynaud et al., 2019). Medetomidine preserves neural activity and vascular response better than isoflurane (Grandjean et al., 2014; Pawela et al., 2009; Weber et al., 2006). The rat head was fixed using a homemade holder with a bite bar and ear bars to minimize the head motion, and body temperature and breathing rate were continuously monitored. At the end of the scanning sessions, rats were woken up with an intra-muscular injection of antagonist atipamezole (0.5 mg/kg) and returned to their cages.

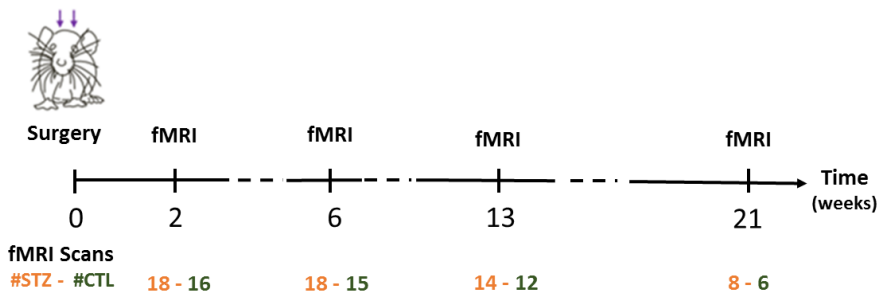


Figure 1. Time line of experiments. Two fMRI runs were acquired per rat for each experiment.

2.2. MRI acquisition

MRI experiments were conducted on a 14.1 T small animal Varian system (Varian Inc.) equipped with 400 mT/m gradients, using an in-house built quadrature surface transceiver.

An anatomical reference scan was acquired using a fast spin-echo multi-slice sequence with following parameters: TE/TR = 10.17/3000 ms, ETL = 4, TEeff = 10.17 ms, field of view (FOV) = 19.2 × 19.2 mm², matrix = 128 × 128, in-plane resolution = 150 × 150 μm², number of slices = 30, thickness = 0.5 mm. Before running the fMRI sequence, anesthesia was switched from isoflurane to medetomidine. The fMRI acquisitions were started after a fixed duration (~ 1 hour) since the switch from isoflurane to medetomidine to minimize between-animal anesthesia-related confounds. Rs-fMRI data were acquired using a two-shot gradient-echo EPI sequence as follows: TE = 10 ms, TR = 800 ms, TR_{vol} = 1.6 s, FOV = 23 × 23 mm², matrix = 64 × 64, in-plane resolution = 360 × 360 μm², 8 slices, thickness = 1.12 mm, 370 repetitions (~ 10 minutes). Two fMRI runs were acquired for each rat. A short scan with 10 repetitions and reversed phase-encoding direction was also acquired to correct for EPI-related geometric distortions.

2.3. fMRI data pre-processing

Images were first skull-stripped automatically using BET (Brain Extraction Tool; FSL, <https://fsl.fmrib.ox.ac.uk/fsl>) (Smith, 2002) and fMRI timeseries were denoised using MP-PCA with a 5x5x5 voxel sliding kernel (Veraart et al.,

2016). The quality of MP-PCA denoising was assessed by inspecting the normality of the residuals (original - denoised) and the temporal signal-to-noise ratio (tSNR) changes before and after denoising. Specifically, the normality of the residuals was tested by the linearity of the relationship between the natural logarithm of the residual distribution probability and the squares of multiple residual standard deviation. Then, the datasets went through EPI distortion correction using FSL's topup (Smith et al., 2004), slice-timing correction (Calhoun et al., 2000; Henson et al., 1999; Sladky et al., 2011), and spatial smoothing (Gaussian kernel: 0.36x0.36x1 mm³). Corrected fMRI images were registered to the Waxholm Space Atlas of the rat brain (<https://www.nitrc.org/projects/whs-sd-atlas>) using linear and non-linear registration in FSL (Jenkinson et al., 2002) and 28 atlas-defined ROIs (14 per hemisphere) were automatically segmented.

Finally, single-session ICA was performed on fMRI timecourses using FSL's MELODIC (Beckmann and Smith, 2004) with high-pass temporal filtering ($f > 0.01$ Hz) and 40 independent components (IC's).

2.4. FIX training

Datasets were randomly split into two groups: a training dataset for FIX (n=49) and a test dataset (n=58). The ICA components in the training dataset were manually classified to signal or artefact, which was mainly based on thresholded spatial maps because ICA is theoretically more robust in the spatial than in the temporal domain (Salimi-Khorshidi et al., 2014; Smith et al., 2012). Here we chose an “aggressive” artefact removal (Griffanti et al., 2014) in the training dataset in order to give the trained classifier a margin to be conservative or aggressive via adjusting the threshold fed to it (small thresholds make it conservative).

The performance of the trained classifier in detecting artefactual components was evaluated on the test dataset by comparing the automatic classification of artefactual components with the manual classification. The classification accuracy was characterized in terms of “recall” and “precision” (Powers, 2011), which are defined as the percentage of the correctly predicted artefact components in all actual artefact components and the percentage of the correctly predicted artefact components in all predicted artefact components, respectively.

2.5. Network analysis and global signal regression

After ICA decomposition and classification, the artefact components were regressed out of the 4D pre-processed datasets to obtain “cleaned” rs-fMRI datasets. The cleaned data were used to compute ROI-to-ROI functional connectivity by calculating correlation coefficients between the ROI-averaged time-series of the 28 atlas-defined ROIs, resulting in a 28×28 FC matrix for each rat.

For FIX, we relied on spatial maps rather than timecourses to evaluate artefactual components. In several cases, components displayed sensible spatial distribution to represent a RSN but the power spectrum showed a peak at a frequency which could be attributed to breathing (**Figure 2**) (the breathing rate was recorded for each run

and its aliased frequency within our 0.01 – 0.31 Hz band calculated). These non-neuronal sources which could not be cleaned using FIX also contribute to the global signal. To mitigate their effect, we used partial correlation of ROI-to-ROI timecourses to build FC matrices, with the global signal as the controlling variable. For every pair of ROIs, the partial correlation was implemented by measuring the correlation between their time-series residuals, after each having been adjusted by the global signal regression (Smith et al., 2011).

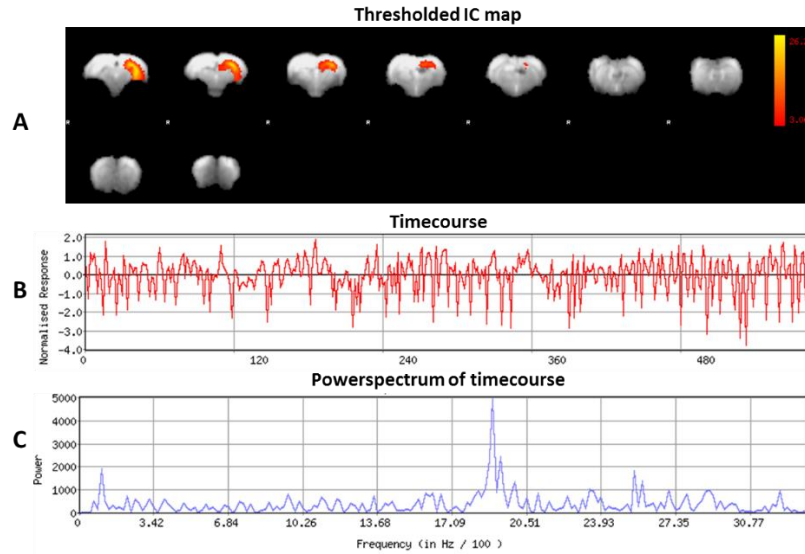


Figure 2. Example of independent component which is anatomically consistent (left hippocampus) yet corrupted by breathing: thresholded spatial map (A), timecourse (B) and the power spectrum of timecourse (C). The power spectrum shows an aliased frequency with a peak at around 0.18 Hz due to breathing.

Finally, statistical comparisons of functional connectivity between STZ and CTL groups at each timepoint were performed using NBS (Zalesky et al., 2010) to identify network connections that showed significant between-group difference. Specifically, NBS uses a two-sample *t*-test to detect differences in group-averaged FC between the two groups. A *t*-statistic threshold was chosen on the basis of medium-to-large sizes of the subnetwork comprised of connections with their *t*-statistic above the threshold (Tsurugizawa et al., 2019). The biggest subnetwork composed of supra-threshold connections was kept for subsequent significance test. Furthermore, significance ($p \leq 0.05$) was family-wise error rate (FWER) corrected using non-parametric permutation ($N = 5000$). Here, four *t*-statistic thresholds (2, 2.15, 2.5, and 3) were selected and compared.

The full data processing pipeline is illustrated in **Figure 3**.

2.6. Data processing pipeline evaluation

To evaluate the rs-fMRI data processing pipeline including MP-PCA denoising (DN), slice-timing correction (SC), spatial smoothing (SM), high-pass filtering (HP), ICA-FIX cleaning (CL) and global signal regression (GSR) in terms

of consistency of within-group functional connectivity in healthy CTL group and in terms of between-group difference, we compared results of the optimized pipeline (DN + SC + SM + HP + CL + GSR, D) with three other processing approaches excluding ICA-FIX cleaning and/or GSR, namely, DN + SC + SM + HP (A), DN + SC + SM + HP + CL (B), and DN + SC + SM + HP + GSR (C), shown in **Table 1**.

Based on the hypothesis that an optimal processing procedure should minimize the variability within the homogeneous group of healthy controls (Zerbi et al., 2015), the within-group variability was assessed by calculating the standard deviation of the Fisher z-transformed correlation coefficients of the FC matrices in the CTL group of healthy rats at each timepoint. In addition, the sensitivity to between-group differences was evaluated by comparing the significant difference in FC between STZ and CTL group at each timepoint.

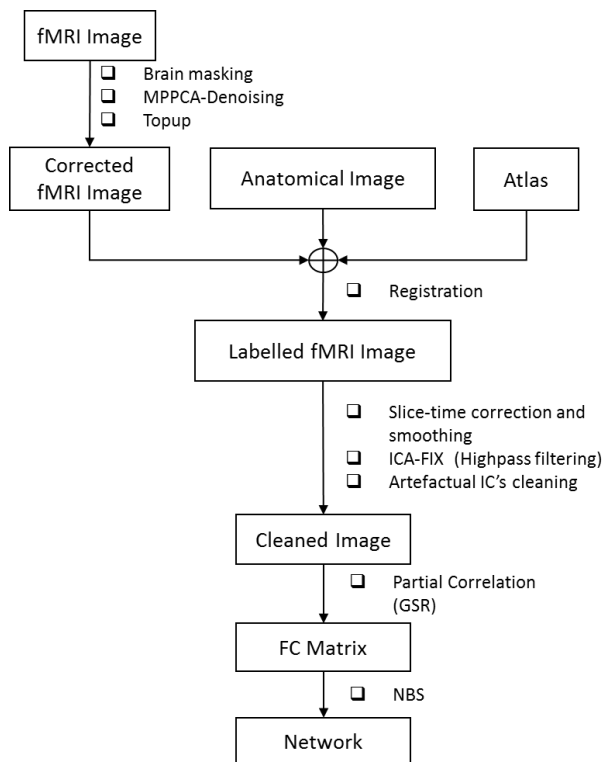


Figure 3. The proposed pipeline for rs-fMRI data processing.

Table 1. The four data processing pipelines and methods they include (“x” – including, “o” – excluding)

Pipelines	MPPCA-denoising (DN)	Slice-timing correction (SC)	Spatial smoothing (SM)	High-pass filtering (HP)	ICA-FIX cleaning (CL)	Global signal regression (GSR)
A	x	x	x	x	o	o
B	x	x	x	x	x	o
C	x	x	x	x	o	x
D	x	x	x	x	x	x

3. Results

A total of 109 rs-fMRI datasets were acquired from 17 rats over 4 timepoints ranging from 2 weeks to 21 weeks. Two datasets were discarded due to bad image quality resulting in 107 datasets left in total. The number of datasets for each group at each timepoint is shown in **Figure 1**. **Figure 4** shows the MR images in one exemplary dataset including the EPI rs-fMRI images, matching anatomical reference and the atlas-based anatomical labels registered to the fMRI images.

3.1. MP-PCA denoising

The average tSNR after MP-PCA denoising improved significantly for all 107 datasets. **Figure 5** shows an example of the average tSNR increase (75.1 to 145.5) over the middle brain slice after MPPCA-denoising. **Figure 6** shows an example of residuals map, histogram, and the normality test. The linearity of $\log(P) = f(r^2)$ confirms the residuals are normally distributed and only Gaussian noise has been removed from the signal.

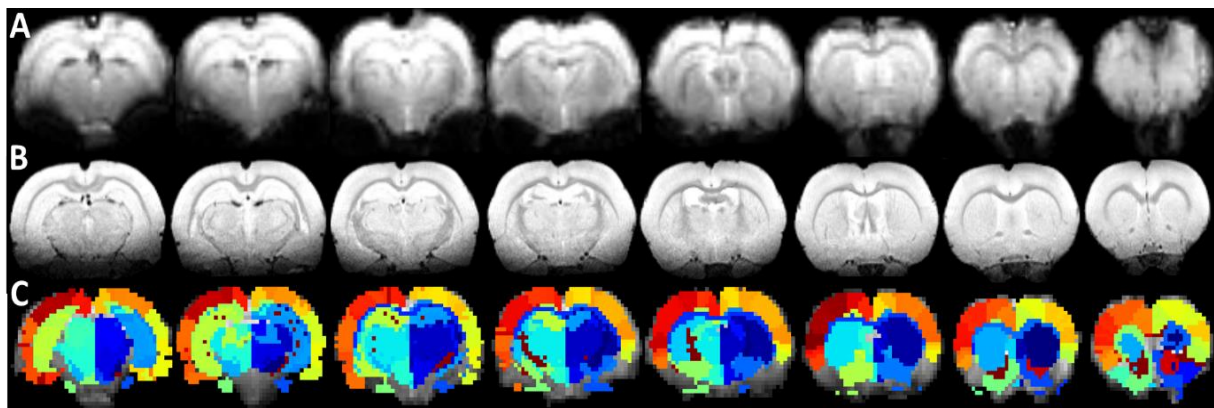


Figure 4. Example of rs-fMRI images of 8 coronal slices (A), matching anatomical MR images (B) and atlas-based anatomical labels registered to the fMRI images (C).

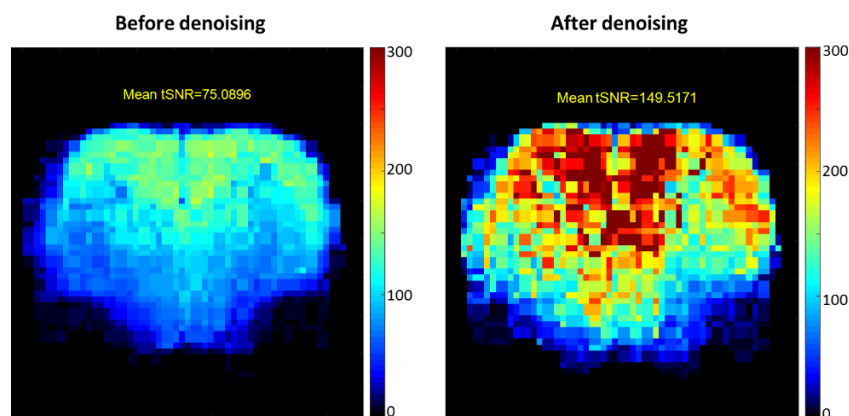


Figure 5. Example of temporal SNR maps, before (left) and after MPPCA-denoising (right). The mean tSNR over the middle brain slice was improved dramatically from 75.1 to 145.5. The SNR profile is typical of a surface coil placed on top of the head, with higher sensitivity in the cortex.

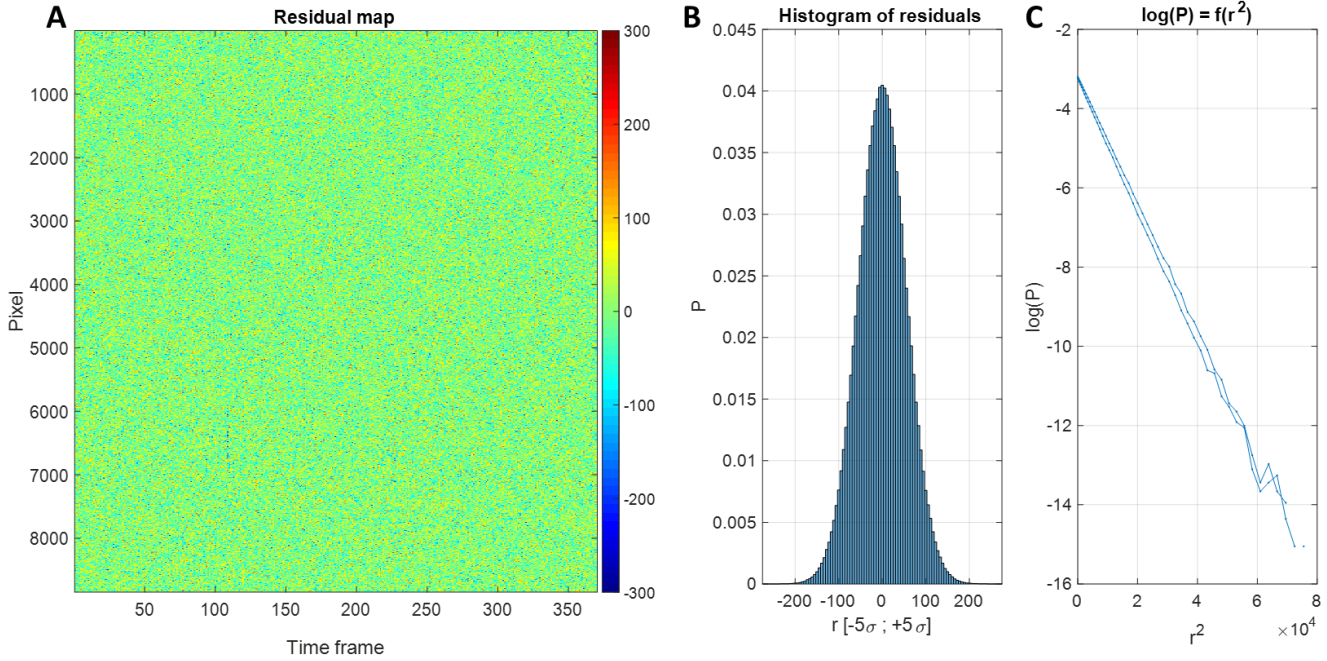


Figure 6. Normality estimation of the residuals after MPPCA-denoising. A: Residuals map of all voxels within the brain mask (rows) and time frame (columns), B: Histogram of residuals, C: Normality test.

3.2. FIX classification

Here, we preferred a lower model order to avoid overfitting (Kuang et al., 2018; Li et al., 2007) and we chose the number of independent components to be 40, which typically explained 90% of the variance. Reaching 95% of explained variance would have required about 90 components, potentially over-splitting networks and making the classification more complicated.

The single-subject ICA was performed on all 107 datasets with 40 components. In the training dataset ($n=49$), 19.8 ± 4.7 components (50 %) were classified as artefacts by hand. In the test dataset ($n=58$), between 40% and 64% of components were classified as artefacts automatically by FIX depending on the threshold. More components could be recognized as artefacts by increasing the FIX threshold at the expense of lowering the classification precision due to more misclassification. Here 45 might be an “optimal” threshold with overall 88% in recall and 90% in precision achieved (Table 2).

Table 2. FIX artefact classification accuracies at different thresholds. Recall = correctly classified artefacts/all real artefacts, precision = correctly classified artefacts/all classified artefacts. As the threshold increases, both the percentage of artefacts detected by FIX and the recall increase but the precision decreases.

FIX THRESHOLD	20	30	40	45	50	60	70
Signal components (%)	44.9	44.9	44.9	44.9	44.9	40.4	36.2
Artefact components (%)	39.6	43.9	49.4	52.7	55.1	59.6	63.8
Unknown components (%)	15.5	11.2	5.7	2.5	0	0	0
FIX artefact recall (%)	69.8	76.5	83.3	87.8	89.7	95.1	98.5
FIX artefact precision (%)	100	95.4	91.6	90.2	86.5	84.4	82.2

3.3. Comparison of pipeline performance

Functional connectivity matrices were calculated based on the 28 atlas ROIs for each of the four data processing approaches.

Our proposed pipeline D (DN+SC+SM+HP+CL+GSR) obtained the minimal within-group variability in the homogeneous group of healthy controls for all timepoints while other procedures excluding CL and/or GSR had higher variability (**Figure 7**), and it also yielded the most consistent and widespread between-group differences at NBS thresholds varying from 2 to 3 (**Figure 8**). No significant difference was found between CTL and STZ group for pipelines without GSR (A and B) regardless of the NBS threshold. Early differences at 2 weeks were shown only using our proposed pipeline D. An NBS threshold of 2.15 revealed group differences at timepoints 2, 13 and 21 weeks. This pattern was consistent with previous reports of acute impairment (2 weeks), transient recovery (6 weeks) and chronic degeneration (13 weeks on) in terms of memory performance (Knezovic et al., 2015) and white matter degeneration (Pereira et al., 2019) in this animal model of Alzheimer's disease. These combined results suggested that artefact cleaning and global signal regression are essential steps for rat rs-fMRI data analysis.

Group differences in FC obtained following data processing according to pipeline D and statistical testing using NBS with a threshold of 2.15 are reproduced in **Figure 9** for more detailed visualization. Brain regions showing altered connectivity in STZ animals were consistent with regions affected by Alzheimer's disease and with previous findings on this animal model (Grieb, 2016; Knezovic et al., 2015; Kraska et al., 2012; Lester-Coll et al., 2006; Mayer et al., 1990; Shoham et al., 2003). At 2 weeks, connections of the anterior cingulate (ACC) to the posterior parietal cortex (PPC), hippocampus (Hip/Sub) and auditory cortex (Au) were primarily affected, particularly in the right hemisphere. At 13 weeks, bilateral changes in connectivity involving ACC, PPC but also striatum (Str) as well as motor (M) and somatosensory (S1, 2) cortices were found. At 21 weeks, connectivity differences were most pronounced, with strong inter-hemispheric alterations in all previously mentioned areas as well as medial temporal lobe (MTL) and retrosplenial cortex (RSC).

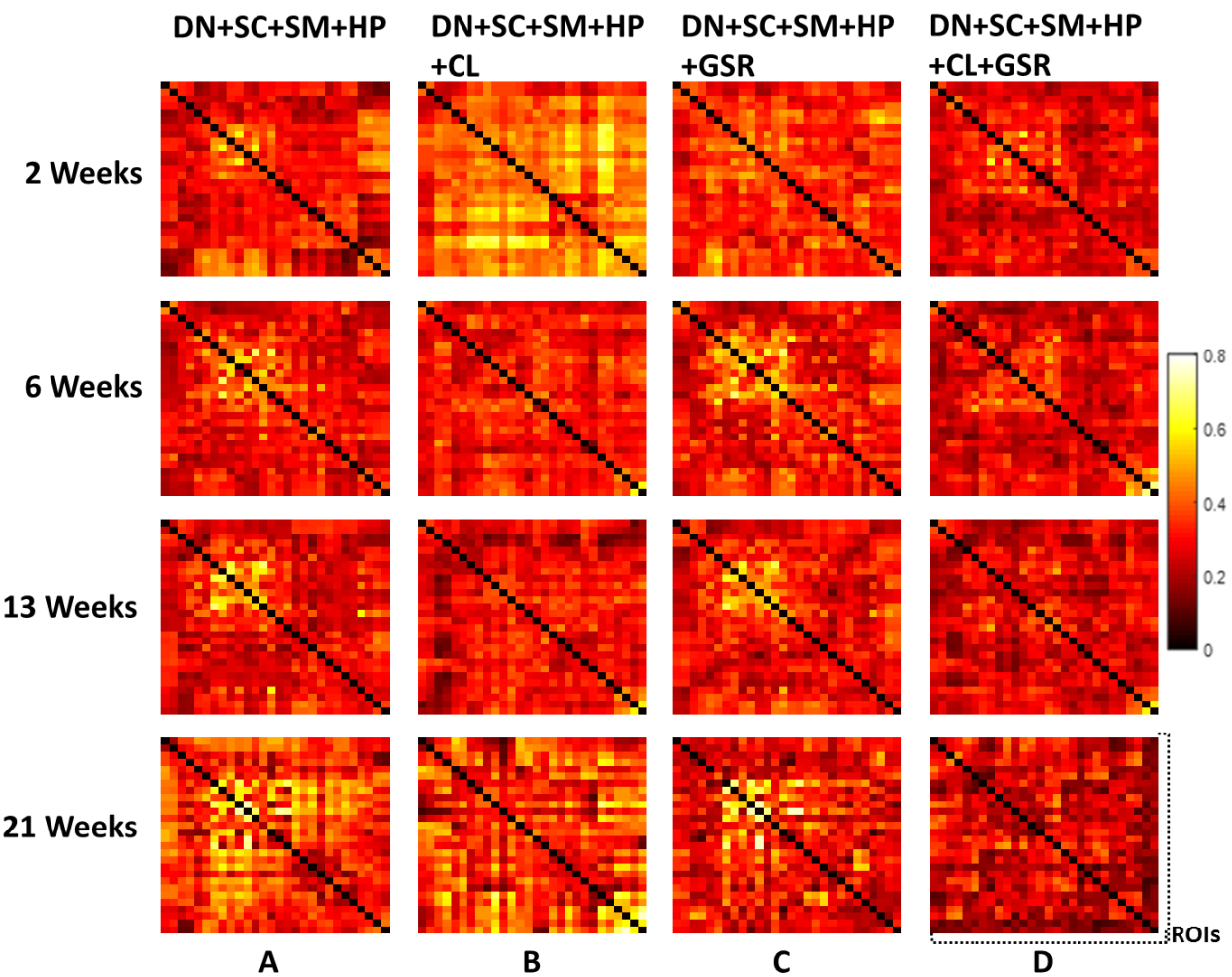


Figure 7. Standard deviation of the Fisher z-transformed correlation coefficient for functional connectivity in the CTL group at four different timepoints for the four pipelines (A-D). Our proposed pipeline D obtained the minimal within-group variability in the homogeneous group of healthy controls for all timepoints while other procedures excluding CL and/or GSR had higher variability

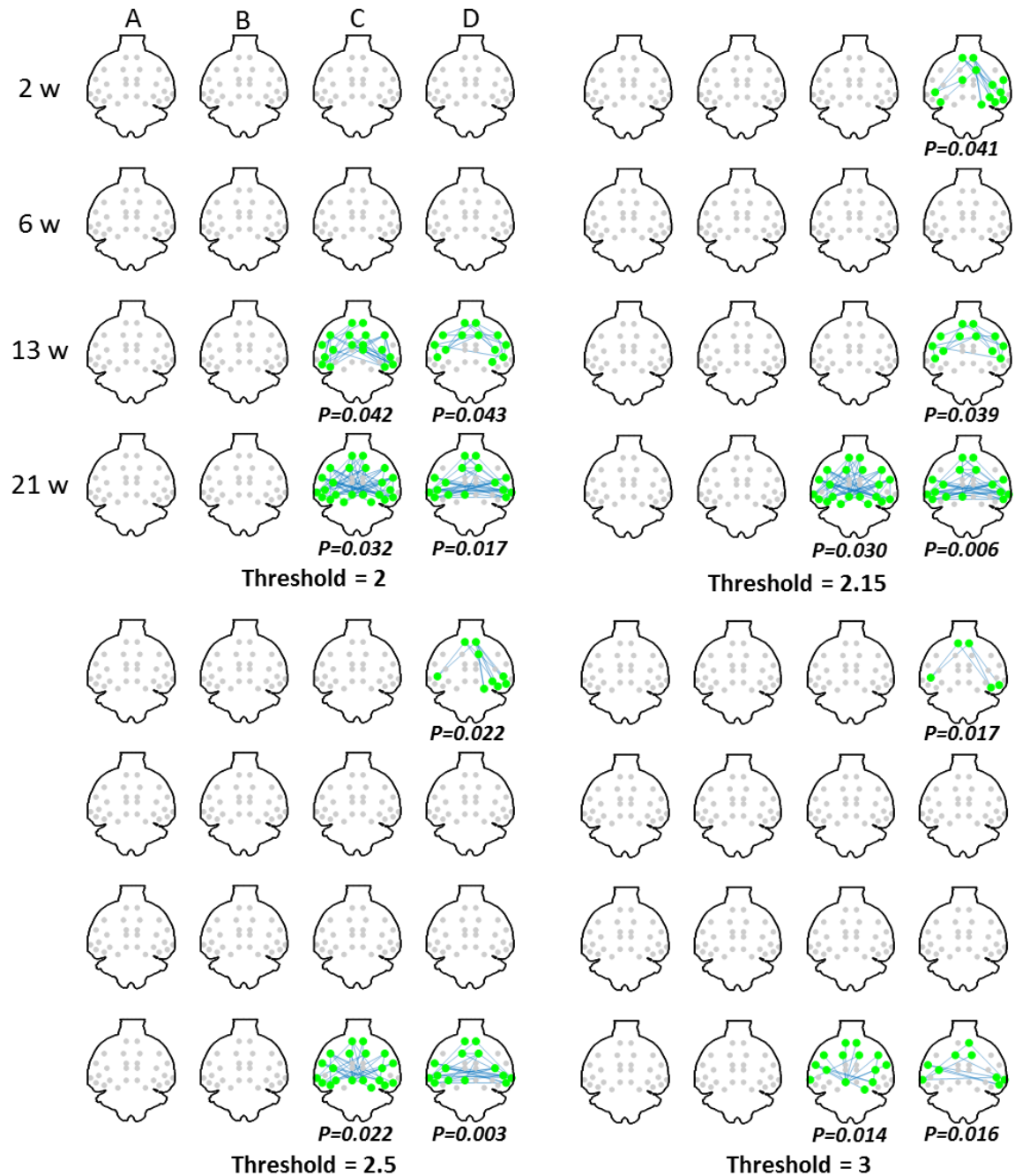


Figure 8. The significant difference in FC between CTL and STZ groups at each timepoints (2, 6, 13 and 21 weeks) for each data processing approach under different NBS thresholds 2, 2.15 2.5 and 3. A: DN+SC+SM+HP, B: DN+SC+SM+HP+CL, C: DN+SC+SM+HP+GSR, D: DN+SC+SM+HP+CL+GSR. Pipeline D yielded the most consistent and widespread between-group differences at NBS thresholds varying from 2 to 3. No significant difference was found between CTL and STZ group for pipelines without GSR (A and B) regardless of the NBS threshold. Early differences at 2 weeks were shown only using our proposed pipeline D.

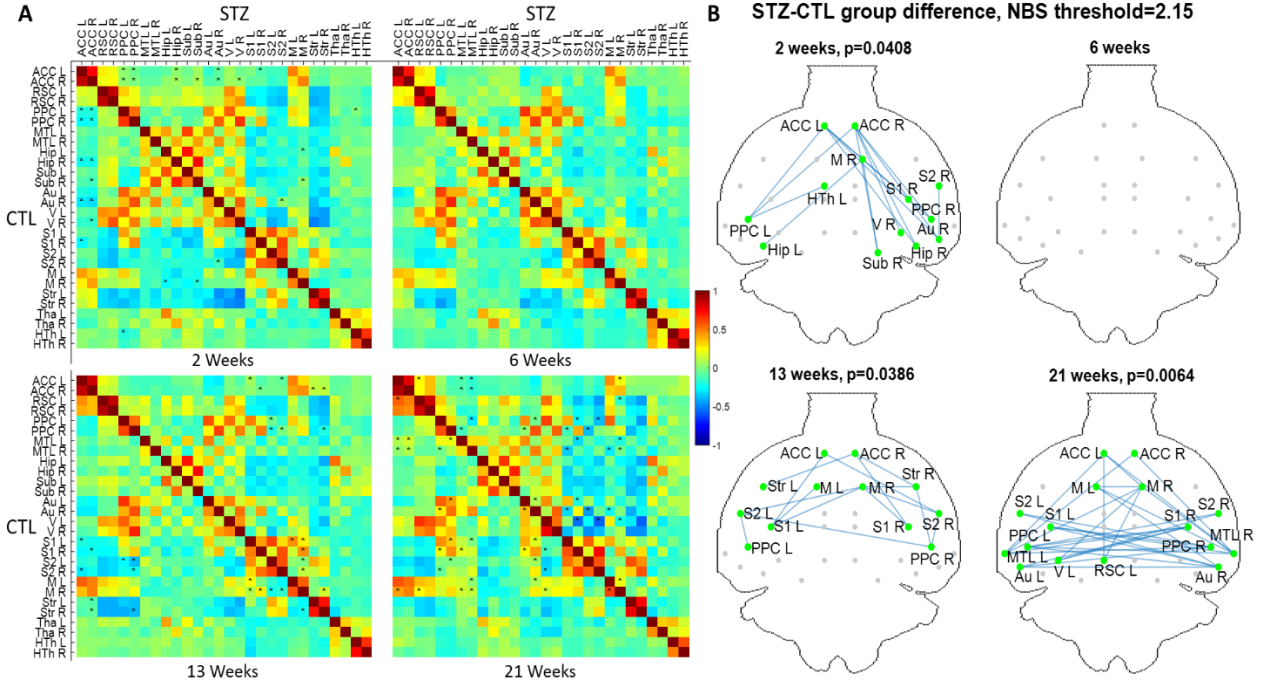


Figure 9. A: Hybrid average FC matrices at each timepoint (top-right half: STZ, bottom-left half: CTL) based on the data processed by the optimized pipeline. *: $p < 0.05$ (FWER corrected) at a threshold of 2.15. B: Graph networks at 4 timepoints. Blue edges and green nodes indicate connections with significant difference. The p-value for each network was given after FWER correction. ACC: anterior cingulate cortex; RSC: retrosplenial cortex; PPC: posterior parietal cortex; MTL: medial temporal lobe; Hipp: hippocampus; Sub: subiculum; Au: auditory; V: visual; S1/S2: primary/secondary somatosensory; M: motor; Str: striatum; Tha: thalamus; HTh: hypothalamus. L/R: left/right.

4. Discussion

In this work, we proposed a resting-state fMRI processing pipeline for rat data. We included a novel thermal noise reduction method based on MP-PCA applied to rs-fMRI data which substantially improved the tSNR. We also built a dedicated FIX ICA classifier for rat brain which, after training, showed a high accuracy in distinguishing artefactual ICA components from the rs-fMRI signal. We evaluated the performance of the pipeline and compared it to two other possible approaches that excluded artefact cleaning and/or global signal regression. We showed that these two steps were essential in minimizing the within-group variability in the healthy control group and in identifying between-group differences in functional connectivity between a control group and a diseased group using the STZ animal model.

The MP-PCA denoising method achieved a high performance in random noise reduction. The residuals followed a Gaussian distribution, showing that MP-PCA is removing thermal noise without affecting structured signal. This method resulted in substantial improvement in tSNR, which helped lay down solid foundations for the subsequent processing. It is often suggested that ICA also has denoising properties. There are two aspects of this statement that should be clarified. On the one hand, if just a few artefactual components are removed from the

signal (as in FIX cleaning), the effect of ICA is primarily to remove structured noise, and not thermal (random) noise. On the other hand, if the ICA decomposition is used to keep and examine just a few independent components that appear anatomically consistent with RSNs, then indeed most of thermal noise is also removed in that process (Beckmann and Smith, 2004). But group-level ICA suffers from its own limitations (Cole et al., 2010) and is not necessarily the appropriate analysis tool for all studies, and seed-based analyses are expected to benefit greatly from prior denoising using MP-PCA. Another study using MP-PCA denoising prior to task fMRI analysis reported an increase of 60% in SNR and improved statistics and extent of the activation areas (Ades-Aron et al., 2019).

Head motion during fMRI acquisitions is one of the major confounding factors that leads to artificial correlation compromising the interpretation of rs-fMRI data (Maknojia et al., 2019; Van Dijk et al., 2012). However, compared to human studies where head motion is common, rodent studies are less impacted by this confound due to the restraining of animals in a fixation setup with ear bars and a bite bar and the use of anesthesia (Pan et al., 2015). In our datasets, no apparent head motion was observed by the visual inspection of time courses except two datasets which were discarded. Motion correction was therefore skipped in the proposed data processing pipeline because it can introduce spurious correlations (Chuang et al., 2019; Grootoorn et al., 2000; Sirmpilatze et al., 2019).

The FIX-based artefact auto-classification has already been applied in human and mouse fMRI datasets (Salimi-Khorshidi et al., 2014; Zerbi et al., 2015). In this work, this automatic artefact removal approach was for the first time implemented for rat data. After being trained in a manually classified dataset, the classifier showed a high accuracy in identifying artefact components from resting state fMRI signal in an untouched test dataset. Nonetheless, **Table 1** shows that there is a trade-off between the recall and precision in the fully automatic classification of artefact components, which means it is not possible to achieve both very high recall and precision with one FIX threshold. However, in practice, this problem could be worked around by half automated classification in which two auto-classifications are first performed with respectively low and high thresholds (20 and 70 for instance) and then the different components between their classified artefacts are manually examined. In this way, by examining a small portion of ICA components (~24%), we are able to achieve a very high classification accuracy in a very short time. We further underline that the training set was cleaned aggressively in order to give flexibility in aggressiveness/conservatism for test datasets by adjusting the threshold. This classifier will be available upon request following publication of the current work. Interestingly, ICA-based cleaning lowered overall intra-group variability at two timepoints (6 weeks and 13 weeks – **Figure 7**) while its effect was less systematic for datasets at 2 and 21 weeks. It did not shed light on any significant differences

between CTL and STZ groups at any timepoint as compared to the minimal protocol A (**Figure 8**, columns A vs B). This suggests ICA-based cleaning is not sufficient for a comprehensive pre-processing pipeline of rat fMRI data.

Although remaining a highly controversial procedure, global signal regression is still commonly used in the analysis of rs-fMRI data (Falahpour et al., 2018) due to its capability of reducing the effects of respiration and motion on functional connectivity estimates (Birn, 2012; Power et al., 2014; Yan et al., 2013) and enhancing the spatial specificity of positive correlations (Fox et al., 2009). More refined approaches similar to GSR are emerging and are certainly also worth exploring (Aquino et al., 2019). Here, we found that pipeline C which included GSR interestingly reduced intra-group variability at timepoints where ICA cleaning was not most effective (2 and 21 weeks) and had little impact on the FC matrix at timepoints when ICA cleaning was most effective (6 and 13 weeks). This suggests the two approaches are complementary and, indeed, protocol D which combines them both reduced most within group variability in the healthy CTL group and revealed most between-group FC differences between the CTL and STZ groups, which were consistent with previous findings in the STZ animal model of Alzheimer's disease.

5. Conclusion

We proposed a new processing pipeline for rat rs-fMRI data which includes MP-PCA denoising, a FIX auto-classification and cleaning of structured artefacts uncovered by ICA, and global signal regression. A new ICA-FIX classifier was built for rat rs-fMRI data which can be readily shared. Importantly, we show that ICA-FIX cleaning and global signal regression each play a critical role in minimizing the within-group variability and in detecting between-group differences. This data processing pipeline for rat rs-fMRI will be made available shortly after publication and will hopefully improve the sensitivity and reproducibility of rs-fMRI studies on rat models of disease and injury.

References

Ades-Aron, B., Veraart, J., Fieremans, E., Novikov, D.S., Shepherd, T.M., 2019. MP-PCA denoising to improve detection of task-based fMRI activation in brain tumor patients, in: Proc. Intl. Soc. Mag. Reson. Med. 28. Montreal, Canada.

Ades-Aron, B., Veraart, J., Kochunov, P., McGuire, S., Sherman, P., Kellner, E., Novikov, D.S., Fieremans, E., 2018. Evaluation of the accuracy and precision of the diffusion parameter EStimation with Gibbs and NoisE removal pipeline. *Neuroimage* 183, 532–543. <https://doi.org/10.1016/j.neuroimage.2018.07.066>

Aquino, K.M., Fulcher, B.D., Parkes, L., Sabaroedin, K., Fornito, A., 2019. Identifying and removing widespread signal deflections from fMRI data: Rethinking the global signal regression problem. *bioRxiv* 662726. <https://doi.org/10.1101/662726>

Bajic, D., Craig, M.M., Mongerson, C.R.L., Borsook, D., Becerra, L., 2017. Identifying Rodent Resting-State Brain Networks with Independent Component Analysis. *Front. Neurosci.* 11. <https://doi.org/10.3389/fnins.2017.00685>

Beckmann, C.F., Smith, S.M., 2004. Probabilistic independent component analysis for functional magnetic resonance imaging. *IEEE Trans. Med. Imaging* 23, 137–152. <https://doi.org/10.1109/TMI.2003.822821>

Birn, R.M., 2012. The role of physiological noise in resting-state functional connectivity. *NeuroImage*, 20 YEARS OF fMRI 62, 864–870. <https://doi.org/10.1016/j.neuroimage.2012.01.016>

Birn, R.M., Diamond, J.B., Smith, M.A., Bandettini, P.A., 2006. Separating respiratory-variation-related fluctuations from neuronal-activity-related fluctuations in fMRI. *NeuroImage* 31, 1536–1548. <https://doi.org/10.1016/j.neuroimage.2006.02.048>

Biswal, B., Yetkin, F.Z., Haughton, V.M., Hyde, J.S., 1995. Functional connectivity in the motor cortex of resting human brain using echo-planar MRI. *Magn. Reson. Med.* 34, 537–541. <https://doi.org/10.1002/mrm.1910340409>

Buckner, R.L., Krienen, F.M., Yeo, B.T.T., 2013. Opportunities and limitations of intrinsic functional connectivity MRI. *Nat. Neurosci.* 16, 832–837. <https://doi.org/10.1038/nn.3423>

Caballero-Gaudes, C., Reynolds, R.C., 2017. Methods for cleaning the BOLD fMRI signal. *NeuroImage*, Cleaning up the fMRI time series: Mitigating noise with advanced acquisition and correction strategies 154, 128–149. <https://doi.org/10.1016/j.neuroimage.2016.12.018>

Calhoun, V.D., Golay, X., Pearlson, G., n.d. Improved fMRI Slice Timing Correction: Interpolation Errors and Wrap Around Effects 1.

Chuang, K.-H., Lee, H.-L., Li, Z., Chang, W.-T., Nasrallah, F.A., Yeow, L.Y., Singh, K.K.D. /O. R., 2019. Evaluation of nuisance removal for functional MRI of rodent brain. *NeuroImage* 188, 694–709. <https://doi.org/10.1016/j.neuroimage.2018.12.048>

Cole, D.M., Smith, S.M., Beckmann, C.F., 2010. Advances and Pitfalls in the Analysis and Interpretation of Resting-State fMRI Data. *Front. Syst. Neurosci.* 4. <https://doi.org/10.3389/fnsys.2010.00008>

Damoiseaux, J.S., Rombouts, S. a. R.B., Barkhof, F., Scheltens, P., Stam, C.J., Smith, S.M., Beckmann, C.F., 2006. Consistent resting-state networks across healthy subjects. *Proc. Natl. Acad. Sci. U. S. A.* 103, 13848–13853. <https://doi.org/10.1073/pnas.0601417103>

Does, M.D., Olesen, J.L., Harkins, K.D., Serradas-Duarte, T., Gochberg, D.F., Jespersen, S.N., Shemesh, N., 2019. Evaluation of principal component analysis image denoising on multi-exponential MRI relaxometry. *Magn Reson Med* 81, 3503–3514. <https://doi.org/10.1002/mrm.27658>

Falahpour, M., Nalci, A., Liu, T.T., 2018. The Effects of Global Signal Regression on Estimates of Resting-state BOLD fMRI and EEG Vigilance Correlations. *bioRxiv* 433912. <https://doi.org/10.1101/433912>

Fornito, A., Bullmore, E.T., 2010. What can spontaneous fluctuations of the blood oxygenation-level-dependent signal tell us about psychiatric disorders? *Curr. Opin. Psychiatry* 23, 239–249. <https://doi.org/10.1097/YCO.0b013e328337d78d>

Fox, M.D., Greicius, M., 2010. Clinical applications of resting state functional connectivity. *Front. Syst. Neurosci.* 4, 19. <https://doi.org/10.3389/fnsys.2010.00019>

Fox, M.D., Raichle, M.E., 2007. Spontaneous fluctuations in brain activity observed with functional magnetic resonance imaging. *Nat. Rev. Neurosci.* 8, 700–711. <https://doi.org/10.1038/nrn2201>

Fox, M.D., Zhang, D., Snyder, A.Z., Raichle, M.E., 2009. The global signal and observed anticorrelated resting state brain networks. *J. Neurophysiol.* 101, 3270–3283. <https://doi.org/10.1152/jn.90777.2008>

Grandjean, J., Schroeter, A., Batata, I., Rudin, M., 2014. Optimization of anesthesia protocol for resting-state fMRI in mice based on differential effects of anesthetics on functional connectivity patterns. *Neuroimage* 102 Pt 2, 838–47. <https://doi.org/10.1016/j.neuroimage.2014.08.043>

Grieb, P., 2016. Intracerebroventricular Streptozotocin Injections as a Model of Alzheimer's Disease: in Search of a Relevant Mechanism. *Mol Neurobiol* 53, 1741–1752. <https://doi.org/10.1007/s12035-015-9132-3>

Griffanti, L., Dipasquale, O., Laganà, M.M., Nemni, R., Clerici, M., Smith, S.M., Baselli, G., Baglio, F., 2015. Effective artifact removal in resting state fMRI data improves detection of DMN functional connectivity alteration in Alzheimer's disease. *Front. Hum. Neurosci.* 9, 449. <https://doi.org/10.3389/fnhum.2015.00449>

Griffanti, L., Salimi-Khorshidi, G., Beckmann, C.F., Auerbach, E.J., Douaud, G., Sexton, C.E., Zsoldos, E., Ebmeier, K.P., Filippini, N., Mackay, C.E., Moeller, S., Xu, J., Yacoub, E., Baselli, G., Ugurbil, K., Miller, K.L., Smith, S.M., 2014. ICA-based artefact removal and accelerated fMRI acquisition for improved resting state network imaging. *NeuroImage* 95, 232–247. <https://doi.org/10.1016/j.neuroimage.2014.03.034>

Grootoonk, S., Hutton, C., Ashburner, J., Howseman, A.M., Josephs, O., Rees, G., Friston, K.J., Turner, R., 2000. Characterization and correction of interpolation effects in the realignment of fMRI time series. *NeuroImage* 11, 49–57. <https://doi.org/10.1006/nimg.1999.0515>

Henson, R., Büchel, C., Josephs, O., Friston, K., 1999. The slice-timing problem in event-related fMRI. *NeuroImage* 9.

Jenkinson, M., Bannister, P., Brady, M., Smith, S., 2002. Improved Optimization for the Robust and Accurate Linear Registration and Motion Correction of Brain Images. *NeuroImage* 17, 825–841. <https://doi.org/10.1006/nimg.2002.1132>

Kasper, L., Bollmann, S., Diaconescu, A.O., Hutton, C., Heinze, J., Iglesias, S., Hauser, T.U., Sebold, M., Manjaly, Z.-M., Pruessmann, K.P., Stephan, K.E., 2017. The PhysIO Toolbox for Modeling Physiological Noise in fMRI Data. *J. Neurosci. Methods* 276, 56–72. <https://doi.org/10.1016/j.jneumeth.2016.10.019>

Knezovic, A., Osmanovic-Barilar, J., Curlin, M., Hof, P.R., Simic, G., Riederer, P., Salkovic-Petrisic, M., 2015. Staging of cognitive deficits and neuropathological and ultrastructural changes in streptozotocin-induced rat model of Alzheimer's disease. *J Neural Transm Vienna* 122, 577–92. <https://doi.org/10.1007/s00702-015-1394-4>

Kraska, A., Santin, M.D., Dorieux, O., Joseph-Mathurin, N., Bourrin, E., Petit, F., Jan, C., Chaigneau, M., Hantraye, P., Lestage, P., Dhenain, M., 2012. In vivo cross-sectional characterization of cerebral alterations induced by intracerebroventricular administration of streptozotocin. *PLoS One* 7, e46196. <https://doi.org/10.1371/journal.pone.0046196>

Kruger, G., Glover, G.H., 2001. Physiological noise in oxygenation-sensitive magnetic resonance imaging. *Magn. Reson. Med.* 46, 631–637. <https://doi.org/10.1002/mrm.1240>

Kuang, L.-D., Lin, Q.-H., Gong, X.-F., Cong, F., Sui, J., Calhoun, V.D., 2018. Model order effects on ICA of resting-state complex-valued fMRI data: Application to schizophrenia. *J. Neurosci. Methods* 304, 24–38. <https://doi.org/10.1016/j.jneumeth.2018.02.013>

Lester-Coll, N., Rivera, E.J., Soscia, S.J., Doiron, K., Wands, J.R., de la Monte, S.M., 2006. Intracerebral streptozotocin model of type 3 diabetes: relevance to sporadic Alzheimer's disease. *J Alzheimers Dis* 9, 13–33.

Li, Y.-O., Adali, T., Calhoun, V.D., 2007. Estimating the number of independent components for functional magnetic resonance imaging data. *Hum. Brain Mapp.* 28, 1251–1266. <https://doi.org/10.1002/hbm.20359>

Liu, T.T., Nalci, A., Falahpour, M., 2017. The global signal in fMRI: Nuisance or Information? *NeuroImage* 150, 213–229. <https://doi.org/10.1016/j.neuroimage.2017.02.036>

Maknojia, S., Churchill, N.W., Schweizer, T.A., Graham, S.J., 2019. Resting State fMRI: Going Through the Motions. *Front. Neurosci.* 13. <https://doi.org/10.3389/fnins.2019.00825>

Mayer, G., Nitsch, R., Hoyer, S., 1990. Effects of changes in peripheral and cerebral glucose metabolism on locomotor activity, learning and memory in adult male rats. *Brain Res* 532, 95–100.

McKeown, M.J., Hansen, L.K., Sejnowski, T.J., 2003. Independent component analysis of functional MRI: what is signal and what is noise? *Curr. Opin. Neurobiol.* 13, 620–629.

Murphy, K., Birn, R.M., Bandettini, P.A., 2013. Resting-state fMRI confounds and cleanup. *NeuroImage, Mapping the Connectome* 80, 349–359. <https://doi.org/10.1016/j.neuroimage.2013.04.001>

Murphy, K., Birn, R.M., Handwerker, D.A., Jones, T.B., Bandettini, P.A., 2009. The impact of global signal regression on resting state correlations: Are anti-correlated networks introduced? *NeuroImage* 44, 893–905. <https://doi.org/10.1016/j.neuroimage.2008.09.036>

Murphy, K., Fox, M.D., 2017. Towards a consensus regarding global signal regression for resting state functional connectivity MRI. *NeuroImage* 154, 169–173. <https://doi.org/10.1016/j.neuroimage.2016.11.052>

Pan, W.-J., Billings, J.C.W., Grooms, J.K., Shakil, S., Keilholz, S.D., 2015. Considerations for resting state functional MRI and functional connectivity studies in rodents. *Front. Neurosci.* 9. <https://doi.org/10.3389/fnins.2015.00269>

Pawela, C.P., Biswal, B.B., Hudetz, A.G., Schulte, M.L., Li, R., Jones, S.R., Cho, Y.R., Matloub, H.S., Hyde, J.S., 2009. A protocol for use of medetomidine anesthesia in rats for extended studies using task-induced BOLD contrast and resting-state functional connectivity. *NeuroImage* 46, 1137–1147. <https://doi.org/10.1016/j.neuroimage.2009.03.004>

Pereira, C., Yin, T., Diao, Y., da Silva, A.R., Jelescu, I., 2019. Longitudinal characterization of white matter degeneration in a rat model of brain glucose hypometabolism and sporadic Alzheimer's disease. Presented at the Proc. Int. Soc. Magn. Reson. Med. 27, Montreal, Canada, p. 1484.

Power, J.D., Mitra, A., Laumann, T.O., Snyder, A.Z., Schlaggar, B.L., Petersen, S.E., 2014. Methods to detect, characterize, and remove motion artifact in resting state fMRI. *NeuroImage* 84, 320–341. <https://doi.org/10.1016/j.neuroimage.2013.08.048>

Power, J.D., Schlaggar, B.L., Petersen, S.E., 2015. Recent progress and outstanding issues in motion correction in resting state fMRI. *NeuroImage* 105, 536–551. <https://doi.org/10.1016/j.neuroimage.2014.10.044>

Powers, D., 2011. Evaluation: From Precision, Recall and F-Measure to ROC, Informedness, Markedness & Correlation. *J. Mach. Learn. Technol.* 2, 37–63.

Reynaud, O., da Silva, A.R., Gruetter, R., Jelescu, I.O., 2019. Multi-slice passband bSSFP for human and rodent fMRI at ultra-high field. *J. Magn. Reson.* 305, 31–40. <https://doi.org/10.1016/j.jmr.2019.05.010>

Saad, Z.S., Gotts, S.J., Murphy, K., Chen, G., Jo, H.J., Martin, A., Cox, R.W., 2012. Trouble at Rest: How Correlation Patterns and Group Differences Become Distorted After Global Signal Regression. *Brain Connect.* 2, 25–32. <https://doi.org/10.1089/brain.2012.0080>

Salimi-Khorshidi, G., Douaud, G., Beckmann, C.F., Glasser, M.F., Griffanti, L., Smith, S.M., 2014. Automatic denoising of functional MRI data: Combining independent component analysis and hierarchical fusion of classifiers. *NeuroImage* 90, 449–468. <https://doi.org/10.1016/j.neuroimage.2013.11.046>

Shoham, S., Bejar, C., Kovalev, E., Weinstock, M., 2003. Intracerebroventricular injection of streptozotocin causes neurotoxicity to myelin that contributes to spatial memory deficits in rats. *Exp Neurol* 184, 1043–52. <https://doi.org/10.1016/j.expneurol.2003.08.015>

Sirmpilatze, N., Baudewig, J., Boretius, S., 2019. Temporal stability of fMRI in medetomidine-anesthetized rats. *Sci. Rep.* 9, 1–13. <https://doi.org/10.1038/s41598-019-53144-y>

Sladky, R., Friston, K.J., Tröstl, J., Cunningham, R., Moser, E., Windischberger, C., 2011. Slice-timing effects and their correction in functional MRI. *NeuroImage* 58, 588–594. <https://doi.org/10.1016/j.neuroimage.2011.06.078>

Smith, S.M., 2002. Fast robust automated brain extraction. *Hum. Brain Mapp.* 17, 143–155. <https://doi.org/10.1002/hbm.10062>

Smith, S.M., Jenkinson, M., Woolrich, M.W., Beckmann, C.F., Behrens, T.E.J., Johansen-Berg, H., Bannister, P.R., De Luca, M., Drobniak, I., Flitney, D.E., Niazy, R.K., Saunders, J., Vickers, J., Zhang, Y., De Stefano, N.,

Brady, J.M., Matthews, P.M., 2004. Advances in functional and structural MR image analysis and implementation as FSL. *NeuroImage* 23 Suppl 1, S208-219.
<https://doi.org/10.1016/j.neuroimage.2004.07.051>

Smith, S.M., Miller, K.L., Moeller, S., Xu, J., Auerbach, E.J., Woolrich, M.W., Beckmann, C.F., Jenkinson, M., Andersson, J., Glasser, M.F., Essen, D.C.V., Feinberg, D.A., Yacoub, E.S., Ugurbil, K., 2012. Temporally-independent functional modes of spontaneous brain activity. *Proc. Natl. Acad. Sci.* 109, 3131–3136.
<https://doi.org/10.1073/pnas.1121329109>

Smith, S.M., Miller, K.L., Salimi-Khorshidi, G., Webster, M., Beckmann, C.F., Nichols, T.E., Ramsey, J.D., Woolrich, M.W., 2011. Network modelling methods for fMRI. *NeuroImage* 54, 875–891.
<https://doi.org/10.1016/j.neuroimage.2010.08.063>

Tsurugizawa, T., Djemai, B., Zalesky, A., 2019. The impact of fasting on resting state brain networks in mice. *Sci. Rep.* 9, 1–12. <https://doi.org/10.1038/s41598-019-39851-6>

Van Dijk, K.R.A., Sabuncu, M.R., Buckner, R.L., 2012. The influence of head motion on intrinsic functional connectivity MRI. *NeuroImage, Neuroergonomics: The human brain in action and at work* 59, 431–438.
<https://doi.org/10.1016/j.neuroimage.2011.07.044>

Veraart, J., Novikov, D.S., Christiaens, D., Ades-aron, B., Sijbers, J., Fieremans, E., 2016. Denoising of diffusion MRI using random matrix theory. *NeuroImage* 142, 394–406.
<https://doi.org/10.1016/j.neuroimage.2016.08.016>

Wang, Y., Li, T.-Q., 2015. Dimensionality of ICA in resting-state fMRI investigated by feature optimized classification of independent components with SVM. *Front. Hum. Neurosci.* 9.
<https://doi.org/10.3389/fnhum.2015.00259>

Weber, R., Ramos-Cabrer, P., Wiedermann, D., van Camp, N., Hoehn, M., 2006. A fully noninvasive and robust experimental protocol for longitudinal fMRI studies in the rat. *NeuroImage* 29, 1303–10.
<https://doi.org/10.1016/j.neuroimage.2005.08.028>

Yan, C.-G., Cheung, B., Kelly, C., Colcombe, S., Craddock, R.C., Di Martino, A., Li, Q., Zuo, X.-N., Castellanos, F.X., Milham, M.P., 2013. A comprehensive assessment of regional variation in the impact of head micromovements on functional connectomics. *NeuroImage* 76, 183–201.
<https://doi.org/10.1016/j.neuroimage.2013.03.004>

Zalesky, A., Fornito, A., Bullmore, E.T., 2010. Network-based statistic: Identifying differences in brain networks. *NeuroImage* 53, 1197–1207. <https://doi.org/10.1016/j.neuroimage.2010.06.041>

Zerbi, V., Grandjean, J., Rudin, M., Wenderoth, N., 2015. Mapping the mouse brain with rs-fMRI: An optimized pipeline for functional network identification. *NeuroImage* 123, 11–21.
<https://doi.org/10.1016/j.neuroimage.2015.07.090>